A Phase Shift Full Bridge Converter with Information Integrated for Battery Charger

Ruwen Wang[1], Siyu Tong[1], Qingfeng Zhang[1] and Yu Chen[1]
[1] School of Electrical and Electronic Engineering, Huazhong University of Science and Technology, Wuhan, China

***Abstract*-- Bidirectional communication between the battery charger and the Lithium-ion batteries is very important to ensure the safe operation of batteries. There is a trend towards the elimination of communication lines by means of wireless technology. Noticing that the information from the charger to the battery (C2B) is simple logic signals 0 or 1, this paper proposes an idea to integrate the information directly into the power transfer path of the battery charger with phase shift full bridge structure, to save hardware cost. The information is converted to senary data and integrated into the charger through the frequency-shift modulation and the phase-shift modulation. The logical information is then demodulated by the controllers on the battery side. The proposed method achieves the C2B information transmission with no extra hardware cost and little negative effect on the charging process. The effectiveness is verified by experiments.**

***Index Terms*-- battery charger, data integration, data transmission, phase shift full bridge.**

I. Introduction

Lithium-ion battery is an excellent energy storage component with high power density and long life. Since its voltage and capacity is very small, it is common to form a battery pack by series and parallel connections. Nowadays, such a series and parallel structure has been widely used in high-power scenarios like electric vehicles and energy storage system [1][2]. However, the batteries should prevent overcharge, overdischarge and overtemperature to avoid lifecycle reduce or explosion [3], hence, it is essential to monitor the voltage, current and the temperature of the cells, and then cutoff the abnormal batteries in time.

For the purpose above, the bidirectional communication between the battery charger (BC) and the batteries is essential to guarantee the batteries working in the safe operation range [4][5]. The communication can be achieved through the communication lines. However, it increases the size and complexity of the system. To eliminate the lines, it is a trend to apply bidirectional wireless communication [5][6]. As Fig. 1(a) shows, the isolated BC charges the battery pack, which is formed by several battery modules in parallel connection by switches S_{ci}. Among each battery module, a module management unit (MMU), with controller inside, measures the voltage, current, temperature of the series connected cells, and

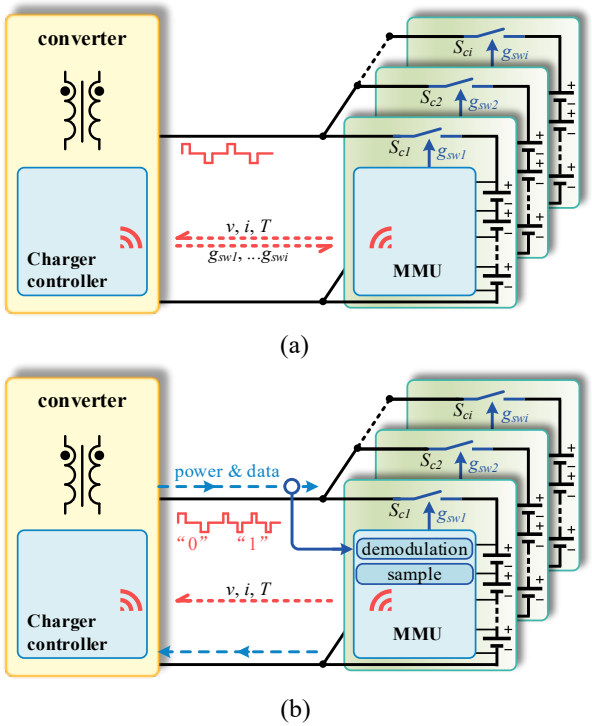

Fig. 1 (a) Bidirectional wireless communication method between charger and battery and (b) proposed method.

sends the information to BC. Meanwhile, the MMU also receives the information from BC to drive the switch S_{ci}, so that the abnormal module can be disconnected from the pack. With this frame, the battery management strategy can be disposed in the BC, and the battery modules can be easily added for capacity extension.

For the information transmitted from the battery to charger (B2C), wireless transmission is cost-efficient since the data sent by the battery modules is numerous and complicated. However, the information transmitted from the opposite direction, i.e., from charger to battery (C2B) is simple and mainly used to control the switches S_{ci}. However, since the wireless receivers are required for the batteries to receive the information, the cost increases with the increase of the battery modules. Therefore, this paper proposes to transmit the information from C2B side through the power transfer path of the BC directly to decrease the cost and size, as Fig. 1(b) shows.

Much research has been conducted to utilize the converter to transmit power and data simultaneously, which helps to achieve this goal [7][8]. For example, [9]

This work is supported by The Young Top-notch Talent Cultivation Program of Hubei Province.

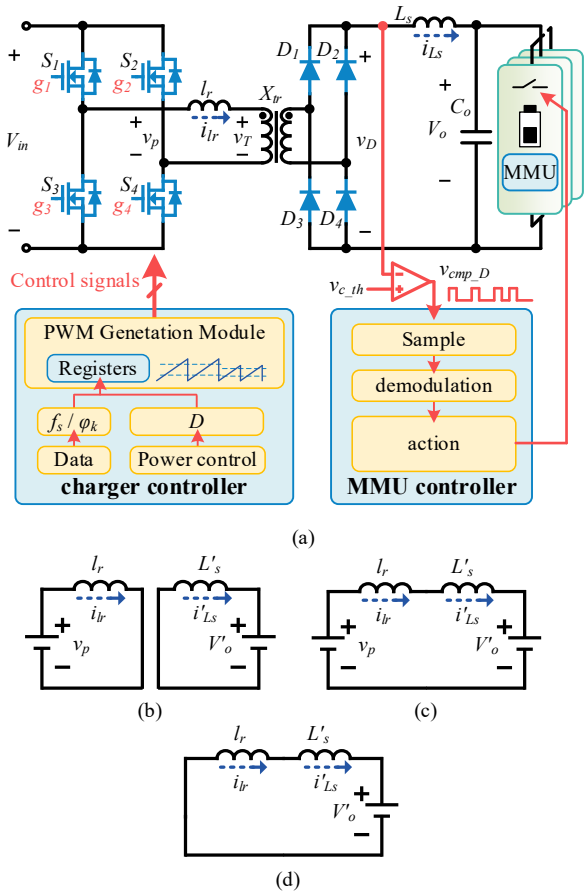

Fig. 2 PSFB converter with information integrated and its equivalent circuit models

proposed to integrate the data into the flyback converter through adjusting the frequency, and demodulate the data by counting the oscillations. However, flyback is not suitable for high-power scenario. For high-power scenario, phase shift full bridge (PSFB) converter has been widely used as BC [10][11]. Ref. [12] integrated the data into the waveform of the transformer through adjusting the width of PWM. The information can be easily demodulated Nevertheless, the converter is worked under discontinuous current mode (DCM) mode which is not suitable for high-power scenarios. Ref. [13] integrated the data into the PSFB converter through the phase-shift modulation, however, the information is demodulated by analyzing the voltage spectrum, which is complicated, requiring the high-performance controller and still increasing the cost.

This paper proposes a data transmission method to integrate the C2B information into the power charging path. The BC is based on a PSFB converter working under continuous current mode (CCM). The information is converted to senary data and integrated through the frequency-shift modulation and the phase-shift modulation, meanwhile, sampled and demodulated by the MMU on the battery side. The proposed method is simple and low-cost, with little negative effect on charging process. In the following, the data modulation and demodulation methods are explained in section II. The experimental results are given in section III to verify the effectiveness of proposed method. Conclusions are drawn in Section VI.

II. Proposed Data Transmission Method with PSFB

Fig. 2(a) shows the PSFB converter and the phase-shift control is utilized with S_1 and S_3 as the leading leg. Fig. 3(a) shows the key waveforms under the normal CCM working mode. T_s is the period, D is the duty cycle and φ_1 and φ_2 are the freewheeling angle of S_3-S_4 and S_1-S_2, respectively, $\varphi_1=\varphi_2$ is satisfied in the normal working mode. The waveform of the output of uncontrolled rectifier v_D can be approximated to the green pulse when the leakage inductor l_r is much less than L'_s (the value of the output inductor L_s converted to the primary side). Therefore, the output voltage V_o can be expressed as [13]:

$$V_o = \frac{2D_{sec}V_{in}}{N} \tag{1}$$

where V_{in} is the input voltage, N is the turn ratio of the transformer X_{tr}, D_{sec} is the effective duty cycle of v_D, i.e. after deducting the duty-cycle loss D_{loss}. It can be seen that the output voltage is only related to D_{sec}. Hence, the frequency and the phase perturbance φ_k (as shown in Fig. 3(b), defined as $(\varphi_2-\varphi_1)/2$) can be used to integrate data and these two methods are defined as the frequency-shift modulation and the phase-shift modulation, respectively. Moreover, to fully explore the information transmission potential of the PSFB converter and increase the data transmission speed, both of them are utilized to integrate data in this paper.

A. Relationship between the Power and the frequency / phase-shift modulation with D_{loss} considered

To integrate the data into the power transfer path, the relationships between the duty cycle D and the power under the frequency-shift modulation and the phase-shift modulation should be clarified. To work under the CCM operation mode, D should satisfy $D>V'_o/(2V_{in})$, where V'_o is V_o converted to the primary side and satisfies $V'_o=NV_o$. To enhance the accuracy, D_{loss} is considered in the derivation. The switches and diodes are considered as ideal switch and the deadtime is ignored to simplify the analysis.

As Fig. 3(a) shows, before stage I, the current of the primary side i_{lr} is negative and flows through S_1 and S_2 and the current of L_s, i_{Ls} flows through D_2 and D_3 at t_0. $i_{lr}(t_0)=-i_{Ls}(t_0)/N$ is satisfied.

1) Stage I ($t_0 \sim t_1$)

When S_2 turns off, i_{lr} flows through S_1 and S_4, therefore, $v_p=V_{in}$. D_1~D_4 commutates in this stage and the voltage of X_{tr}, v_T, is zero. The equivalent circuit model is shown in Fig. 2(b). i'_{Ls} in this model represents the current i_{Ls} converted to the primary side, which satisfies $i'_{Ls}=i_{Ls}/N$. Hence, the expressions of i_{lr} and i'_{Ls} can be expressed as follows:

$$i_{lr}(t) = i_{lr}(t_0) + \frac{V_{in}}{l_r}(t-t_0) \tag{2}$$

$$i'_{Ls}(t) = i'_{Ls}(t_0) - \frac{V'_o}{L'_s}(t-t_0) = -i_{lr}(t_0) - \frac{V'_o}{L'_s}(t-t_0) \tag{3}$$

where the converted inductor $L'_s=N^2L_s$. This stage ends at t_1 when the commutation ends and $i_{lr}(t_1)=i'_{Ls}(t_1)$, and from this, the duration T_{01} can be obtained by solving equation (2) and (3).

2) Stage II ($t_1 \sim t_2$)

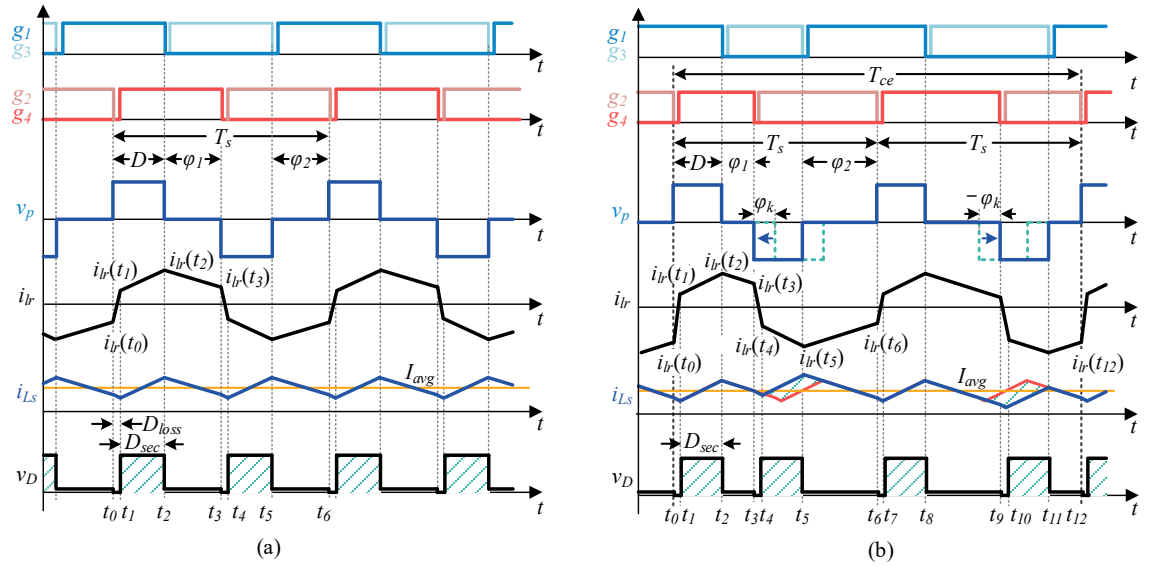

Fig. 3 Key waveforms of (a) the normal working mode and (b) the phase-perturbance working mode

After the commutation of the diodes, the current flows through D_1 and D_4, besides, $i_{lr} = i'_{Ls}$ is satisfied. The equivalent circuit model is shown in Fig. 2(c). Therefore, i_{lr} can be expressed as:

$$i_{lr}(t) = i'_{Ls}(t) = i_{lr}(t_1) + \frac{V_{in} - V'_o}{l_r + L'_s}(t - t_1) \tag{4}$$

This stage ends at t_2 when S_1 turns off and the duration T_{12} is $(DT_s - T_{01})$.

3) Stage III ($t_2 \sim t_3$)

When S_1 turns off at t_2, i_{lr} flows through S_3 and S_4, causing v_p=0. The equivalent circuit model is shown in Fig. 2(d). i_{lr} can be expressed as:

$$i_{lr}(t) = i'_{Ls}(t) = i_{lr}(t_2) + \frac{-V'_o}{l_r + L'_s}(t - t_2) \tag{5}$$

This stage lasts for T_{23}=(1/2-D)T_s.

Since the waveform of i_{lr} is symmetrical in the normal operating mode, the analysis of the half cycle t_0~t_3 is sufficient to show the characteristics. The primary current $i_{lr}(t_3)$ at time t_3 and $i_{lr}(t_0)$ at time t_0 are equal in amplitude and opposite in direction, satisfying $i_{lr}(t_3)$=−$i_{lr}(t_0)$. Combined with equation (2)~(5), the value of i_{lr} at $t_0 \sim t_3$ can be solved and the power P transferred to the battery side in the normal working mode can be expressed as:

$$P = \frac{V_{in}V'_o}{4f_s l_r(l_r + L'_s)(L'_s V_{in} + l_r V'_o)}(-L'^2_s V'_o - 4D^2 l_r^2 V'_o + 2Dl_r^2 V'_o + 2DL'^2_s V_{in} + 2Dl_r L'_s V_{in} - 2Dl_r L'_s V'_o) \tag{6}$$

where f_s is the switching frequency.

As for the phase-perturbance working mode, Fig. 3(b) shows its key waveforms. The phase-perturbance breaks the symmetrical of the working stages, affecting the output voltage, transferred power, and the magnetic balance of X_{tr}. To mitigate the negative effect on the magnetic balance, two switching period with the same frequency are combined together as a new data transmission period T_{ce}, in addition, φ_k and its opposite value are applied to the adjacent switching period as Fig. 3(b) shows. It is worth noting that φ_k should be limited to 0<|φ_k|<(1/2-DT_s) to ensure the normal operation of the circuit and should be carefully chosen considering the resolution of the MMU controller to achieve demodulation.

The introduction of the phase-perturbance angle φ_k and the special design above causing that $i_{lr}(t_3)$ is no longer equal to $-i_{lr}(t_0)$, hence, equation (6) should be modified. Nevertheless, since the structure of the circuit does not change, the phase-perturbance will not change the equation of different working stages. The equations of stage I to stage III is the same as the equation (2)~(5) while the duration of stage III is modified as:

$$T_{23} = = (\frac{1}{2} - D - \frac{\varphi_k}{2\pi})T_s \tag{7}$$

Before the turn off of S_4, $i_{lr}(t_3)$=$i'_{Ls}(t_3)$. $i_{Ls}(t_3)$ flows through D_1 and D_4.

1) Stage IV ($t_3 \sim t_4$)

When S_4 turns off at t_3, i_{lr} flows through S_2 and S_3, and v_p=−V_{in}. Similar to the analysis of stage I, D_1~D_4 commutates in this stage. The equation for this stage is as follows:

$$i_{lr}(t) = i_{lr}(t_3) + \frac{-V_{in}}{l_r}(t - t_3) \tag{8}$$

$$i'_{Ls}(t) = i'_{Ls}(t_3) - \frac{V'_o}{L'_s}(t - t_3) = i_{lr}(t_3) - \frac{V'_o}{L'_s}(t - t_3) \tag{9}$$

The commutation ends at t_4 with $i_{lr}(t_4)$=−$i'_{Ls}(t_4)$. The duration T_{34} can be solved from equation (8) and (9).

2) Stage V ($t_4 \sim t_5$)

After the commutation of the diodes, the current flows through D_2 and D_3 and i_{lr}=−i'_{Ls} is satisfied. i_{lr} can be expressed as:

$$i_{lr}(t) = -i'_{Ls}(t) = i_{lr}(t_4) + \frac{-(V_{in} - V'_o)}{l_r + L'_s}(t - t_0) \tag{10}$$

The duration T_{45} is $(DT_s - T_{34})$.

3) Stage VI ($t_5 \sim t_6$)

When S_3 turns off at t_5, i_{lr} flows through S_1 and S_2, and v_p=0. i_{lr} can be expressed as:

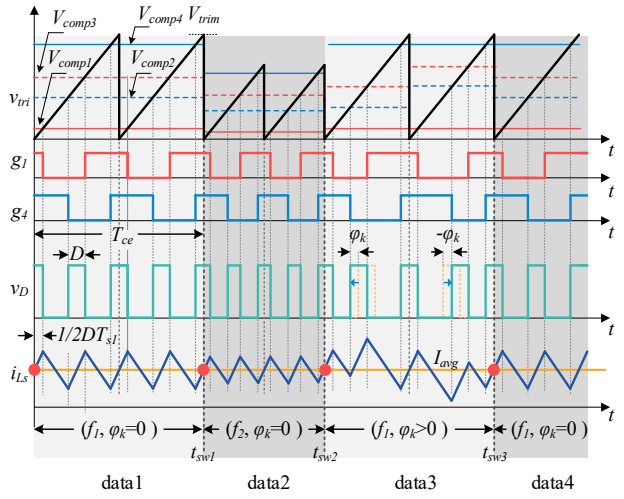

Fig. 4 Working mode switching process.

$$i_{lr}(t) = -i'_{Ls}(t) = i_{lr}(t_5) - \frac{-V'_o}{l_r + L'_s}(t - t_0) \tag{11}$$

This stage lasts for:

$$T_{56} == (\frac{1}{2} - D + \frac{\varphi_k}{2\pi})T_s \tag{12}$$

The analysis of t_6~t_{12} is the same with that of t_0~t_6, while the duration between t_8~t_9 and t_{11}~t_{12} satisfy T_{89}=T_{56} and T_{1112}=T_{23}, respectively. Since $i_{lr}(t_0)$ equals to $i_{lr}(t_{12})$, combining equation (2)~(5) and (7)~(12), i_{lr} at t_0 ~ t_{12} can be solved and the power P_{ps} of the phase-perturbance working mode can be calculated as:

$$\begin{aligned} P_{ps} &= P + \Delta P_{ps} \\ &= P + \frac{-2l_r L'^2_s V_{in} V'^2_o}{f_s(l_r + L'_s)(l_r V'_o + L'_s V_{in})(l_r^2 + L'^2_s)} \cdot \left(\frac{\varphi_k}{2\pi}\right)^2 \end{aligned} \tag{13}$$

where ΔP_{ps} is the power produced by phase perturbance, which is related to the circuit parameters, V_{in}, V_o' and f_s.

Using equations (6) and (13), D can be calculated with given f_s and φ_k to ensure that the desired power can always be transferred.

B. Mode Switch Point Selection and its implementation

As the information is integrated into the different working modes of the converter, the mode switch is unavoidable. When the PSFB converter switches from one working mode to another, it inevitably affects the output current and output voltage. In this paper, the effect is reduced by properly selecting the mode-switching moment. When l_r is much less than L'_s, i_{Ls}, the current of L_s can be approximated as a triangular waveform as shown in Fig. 4, with I_{avg} as its average value. The mode switching moment is selected at the average-current-crossing point, t_{sw}. Fig. 4 shows the mode-switching process and I_{avg} of T_{ce} can keep constant before and after the mode-switching in both modulation methods. To implement the proposed mode switching method, the sawtooth waveform is selected as the carrier waveform since it has unique values corresponding to the time in the period, so that the generation of the control signal can be convenient.

TABLE.I
CORRESPONDENCE BETWEEN WORKING MODES AND DATA

Working state		data
frequency	phase	
f_0	$\varphi_k = 0$	No data/end mark
f_0	$\varphi_k > 0$	Start mark
f_1	$\varphi_k = 0$	0
f_1	$\varphi_k > 0$	1
f_1	$\varphi_k < 0$	2
f_2	$\varphi_k = 0$	3
f_2	$\varphi_k > 0$	4
f_2	$\varphi_k < 0$	5

Detailed generation process of the control signals can refer to Fig. 4.

C. Modulation and Demodulation

The method proposed is a serial transmission method where one code element of data can be transferred per data transmission period T_{ce} and different data are represented by the different working modes of one period T_{ce}. As mentioned above, both of the frequency-shift and the phase-shift modulation are used to integrate data into the power transfer path to achieve the C2B data transmission. hereinafter, two frequencies f_1 and f_2 are selected for the frequency-shift modulation and one phase-perturbance angle is selected for the phase-shift modulation. Two status are formed with two frequencies. However, since T_{ce} is a combination of two switching periods with the same frequency and the opposite phase-perturbance angles, two kinds of status can be formed in the phase-perturbance working mode with one perturbance angel. Therefore, three status can be formed for the phase-shift modulation, namely zero perturbance (φ_k=0), positive perturbance (φ_k>0) and negative perturbance (φ_k<0). Combining the two degrees of freedom, frequency and phase, six kinds of working modes exist, so one code element can transmit senary data (0~5). This method increases the information capacity per code element and can increase the speed of information transmission. The correspondence between the working modes and data is defined in Table I. During the data transmission, the BC controller determines the working modes according to the data and generates corresponding control signals to change the working mode. By this means the information is integrated into the power transfer path.

As for the demodulation, v_D is chosen to demodulate the data. A comparator converts v_D into a pulse signal v_{cmp_D}, which can be directly connected to the MMU controller. After that, the controller captures the pulse edges, counts the pulse intervals, and judges f_s and φ_k to determine the data received.

Furthermore, the structure of the data packet should be predefined for information transmission. An example is given in Fig. 5(a) to control five battery modules. Firstly, when no data transmits, the PSFB converter works with frequency f_0 and φ_k = 0. Once the data is prepared, a unique start mark, formed by the working mode of f_0 and φ_k>0, is sent ahead to mark the beginning of the data. After the start mark, three cell elements are followed to give the address

No data	Start mark	data (senary 0~5)			End mark (no data)
		data 1	data 2	data 3	

data 1 (0~5)	**Address** of the battery module	0	Broadcast
		1	1
		i	*i*
		5	5

data 2 (0~1)	**Action** of the switch	0	Turn off
		1	Turn on

data 3 (0~5)	**Required Data Type**	0	SOC
		1	Temperature
		2	Current
		3	Voltage
		…	…

(a)

2 data (0~5)	**Address** of the battery module	0	Broadcast
		1	1
		…	…
		i_1i_2	$i_1\times 6+i_2$
		55	35

(b)

Fig. 5 (a) An example of the data packet for system with 5 modules and (b) an example of the address coding with 2 code elements of data for address.

i to locate the battery module *i*, the action of the corresponding switch S_{ci}, and the type of data required by the charger side, respectively. When the data transmission finishes, the working mode of f_0 and φ_k=0 is given to mark the end. The start and the end of data is defined to help the MMU controller demodulate the data correctly. With this predefined data packet, the MMU controller can respond to the demand to turn on/off the switch S_{ci} and send corresponding type of data to the charger side by wireless transmission.

It is worth noting that although senary encoding is used for data transmission, the proposed method can also be used in battery pack systems with more than 6 modules through adjust the predefined data packet structure. When applied to a system with more than 6 battery modules, the number of the code element representing address in the data packet must be increased so that each battery module can be located. For example, when 2 code elements are used as the address, the system can control up to 35 (6^2-1) battery modules. The corresponding address coding example is given in Fig. 5(b).

III. Experiment Verification

To verify the effectiveness of the proposed C2B data transmission method, a PSFB converter is built. Its input voltage is 48V and the output voltage is 12V. The battery pack at the output port of the PSFB converter is replaced by capacitors with a resistor connected in parallel as the load, so that proposed C2B data transmission method can be verified quickly. The frequency f_0 when no data transfers takes the value of 66.6kHz and the frequency f_1 and f_2 of the frequency-shift modulation take the value of 100kHz and 80kHz. Considering that the PSFB converter

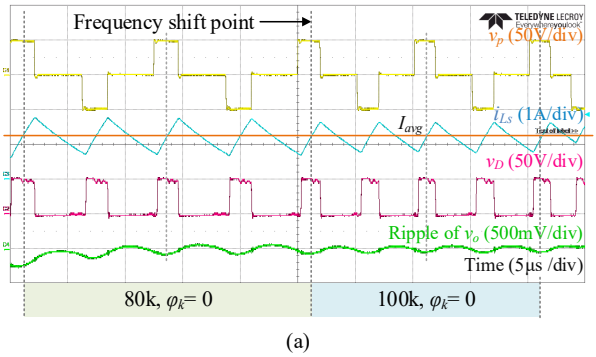

(a)

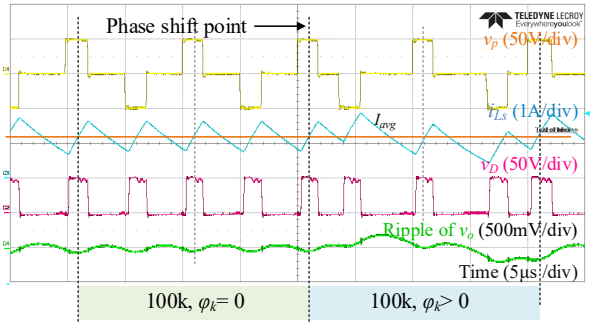

(b)

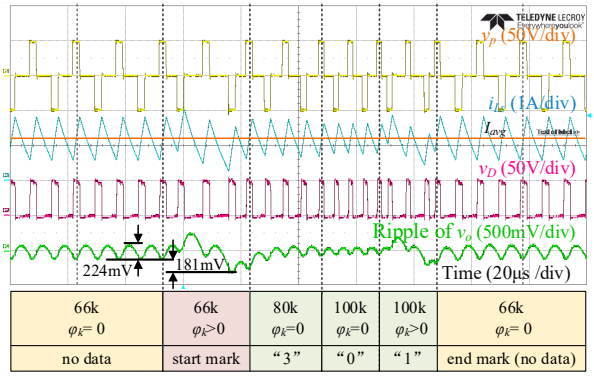

(c)

Fig. 6 Waveforms of (a) mode switch process of frequency shift and (b) phase shift, and (c) data transmission process of ("3", "0", "1")

operates mostly with no data, f_0 is selected to be lower than f_1 and f_2, in order to decrease the switching loss. φ_k takes the value of 0.586rad, 0.880rad and 0.704rad for the frequency f_0, f_1 and f_2, respectively.

Fig. 6(a) shows the mode switch process of the frequency-shift from f_2 to f_1 without phase disturbance. It can be seen that by setting the frequency switch point at the average-current-crossing point, t_{sw}, the average of the inductor current i_{Ls} remains at the average value of I_{avg} before and after the frequency switch. It can be seen that the ripple of the output voltage has no fluctuations when the frequency switch. Fig. 6(b) shows the mode switch process of the phase-shift from zero perturbance φ_k=0 to positive perturbance φ_k>0. This shows that through combining two switching periods with the same frequency and the opposite phase-perturbance angles, the current can return to I_{avg} at the end of the period T_{ce} when the phase-perturbance applied. The average current of i_{Ls} is kept at I_{avg} before and after the phase-shift while the maximum

ripple disturbance resulted from the phase-shift is 103 mV, 0.8% of the output voltage.

Fig. 6(c) shows the waveforms of the data transmission process of one data packet as shown in Fig. 5(a). Three code elements (“3”, “0”, “1”) are sent in one data packet, indicating to turn off S_{c3} to disconnect battery module 3, and send the temperature of battery module 3 to the charger side. It can be seen that the data is integrated into different working modes of the converter, effecting the intervals of the pulse waveform of v_D. Therefore, the MMU controllers can demodulate the data to determine corresponding action. Fig. 6(a) shows that i_{Ls} is not disturbed during the data transmission process. When the converter works under the state with no data transfer, that is, 66k, zero perturbance, the output ripple of the PSFB converter is 224mV, with the ripple coefficient of 1.8%. The maximum value of the ripple disturbance introduced by the information transmission process is 181mV, which appears when transmitting the start mark. Hence, the proposed C2B data transmission method has very little impact on the power transfer. It is worth mentioning that the capacitance of the output capacitor is small in the experiment. However, in the actual scenario of battery charging, the output terminal is connected to the battery pack, therefore, the equivalent capacitance of the output is relatively large and the ripple coefficient can be greatly reduced. The experimental results above have verified the feasibility of the proposed C2B data transmission method.

IV. Conclusions

This paper proposes an information transmission method through the power transfer path of the PSFB converter to replace the wireless data transmission from the charger to the battery (C2B). The information is converted to senary data and integrated into different working modes of the charger through the frequency-shift modulation and the phase-shift modulation. Besides, it is demodulated by the MMU controller on the battery side through sampling the output of the uncontrolled rectifier. The working mode-switching moment is specially selected at the average-current-crossing point to mitigate the effects of mode switching. The proposed method is low cost and has little effect on power transfer.

References

[1] M. A. Hannan, M. M. Hoque, A. Hussain, Y. Yusof, and P. J. Ker, “State-of-the-Art and Energy Management System of Lithium-Ion Batteries in Electric Vehicle Applications: Issues and Recommendations,” *IEEE Access*, vol. 6, pp. 19362–19378, Mar. 2018.

[2] Y. Weng and C. Ababei, “Battery Pack Cell Balancing using Topology Switching and Machine Learning,” *2022 IEEE Vehicle Power and Propulsion Conference, VPPC 2022 - Proceedings*, 2022.

[3] Y. S. Lee and M. W. Cheng, “Intelligent control battery equalization for series connected lithium-ion battery strings,” *IEEE Transactions on Industrial Electronics*, vol. 52, no. 5, pp. 1297–1307, 2005.

[4] C. H. Kim, M. Y. Kim, and G. W. Moon, “A modularized charge equalizer using a battery monitoring ic for series-connected li-ion battery strings in electric vehicles,” *IEEE Transactions on Power Electronics*, vol. 28, no. 8, pp. 3779–3787, 2013.

[5] X. Huang, A. B. Acharya, J. Meng, X. Sui, D. I. Stroe, and R. Teodorescu, “Wireless Smart Battery Management System for Electric Vehicles,” *ECCE 2020 - IEEE Energy Conversion Congress and Exposition*, pp. 5620–5625, 2020.

[6] A. Chon, I. Lee, J. Lee, and M. Lee, “Wireless battery management system (WiBMS),” *Large Lithium Ion Battery Technology and Application Symposium, LLIBTA 2015 - Held at AABC 2015*, pp. 315–320, 2015.

[7] M. Liserre, H. Beiranvand, Y. Leng, R. Zhu, and P. A. Hoeher, “Overview of Talkative Power Conversion Technologies,” *IEEE Open Journal of Power Electronics*, vol. 4, no. February, pp. 1–15, 2023.

[8] C. C. Huang and C. L. Lin, “Wireless Power and Bidirectional Data Transfer Scheme for Battery Charger,” *IEEE Transactions on Power Electronics*, vol. 33, no. 6, pp. 4679–4689, 2018.

[9] G. H. Min and J. I. Ha, “Inner Supply Data Transmission in Quasi-Resonant Flyback Converters for Li-Ion Battery Applications Using Multiplexing Mode,” *IEEE Transactions on Power Electronics*, vol. 34, no. 1, pp. 64–73, 2019.

[10] B. Whitaker *et al.*, “A high-density, high-efficiency, isolated on-board vehicle battery charger utilizing silicon carbide power devices,” *IEEE Transactions on Power Electronics*, vol. 29, no. 5, pp. 2606–2617, May 2014.

[11] M. S. Lee, C. Y. Lim, Y. Jeong, T. W. Kim, and G. W. Moon, “A High Efficiency Phase-Shift Full-Bridge Converter with Improved Clamping Circuit to Eliminate Oscillation for EV Battery Charger,” *2020 IEEE 9th International Power Electronics and Motion Control Conference, IPEMC 2020 ECCE Asia*, pp. 1696–1701, 2020.

[12] R. Zhang, S. Member, and J. Wu, “A Novel Battery Management System Architecture Based on an Isolated Power/Data Multiplexing Transmission Bus,” *IEEE Transactions on Industrial Electronics*, vol. PP, no. c, p. 1, 2018.

[13] J. Du, J. Wu, R. Wang, Z. Lin, and X. He, “DC Power-Line Communication Based on Power/Signal Dual Modulation in Phase Shift Full-Bridge Converters,” *IEEE Transactions on Power Electronics*, vol. 32, no. 1, pp. 693–702, 2017.